Available online at www.sciencedirect.com
SCIENCE DIRECT
Polymer 46 (2005) 9574–9584
polymer
www.elsevier.com/locate/polymer

The effects of intragallery polymerization on the structure of PMMA–clay nanocomposites

Lisa M. Stadtmueller*, Kyle R. Ratinac, Simon P. Ringer

Australian Key Centre for Microscopy and Microanalysis, The University of Sydney, Madsen Building, F09, Sydney, NSW 2006, Australia

Received 15 April 2005; received in revised form 11 August 2005; accepted 12 August 2005
Available online 26 August 2005

Abstract

In situ bulk polymerization of polymethylmethacrylate (PMMA)–clay nanocomposites was initiated with a benzoyl peroxide/amine redox couple at room temperature. This was accomplished with a newly synthesized cationic molecule—containing an aliphatic chain and an aromatic tertiary amine—that was ion exchanged onto the clay surface in order to control the rate of intragallery polymerization relative to that of extragallery polymerization. The rate and location of initiation significantly affected the degree of dispersion of the silicate layers. Accelerating intragallery polymerization of clay with low cation exchange capacity was found to produce the maximum interlayer distance as evident from transmission electron microscope images.

Keywords: Polymethylmethacrylate; Nanocomposite; Clay

1. Introduction

The formation of polymer–clay nanocomposites dramatically enhances the physical and mechanical properties of polymers by dispersing nanoscale silicate platelets throughout a polymer matrix. As much as a 10-fold increase in material strength and modulus has been achieved with dispersion of modest amounts of low-cost, surface-treated montmorillonite clay in epoxy systems [1]. When the clay is well dispersed throughout a polymer matrix, significant improvements to material hardness [2], barrier properties [3], thermal stability [4,5] and flame retardance [6,7] are reported [8]. As a result, this technology has attracted widespread interest and numerous applications have been developed for the automotive, aerospace, packaging, coatings and rubber industries [9].

The clays that commonly are used as the nanoscale filler come from the smectite family of layered silicates. These comprise disk-like platelets or layers—each less than 1 nm in thickness but extending laterally on the order of 300 nm—that are stacked together to form face-to-face tactoids. Each platelet has a negative charge arising from isomorphous substitution in the lattice structure, which is compensated by naturally occurring cations that reside within the gallery (or interlayer) regions between the platelets. These cations can be exchanged with other cations under appropriate conditions, allowing the clay surface to be modified by ion exchanging large, organic cations into the galleries to increase compatibility between the normally hydrophilic clay surfaces and the surrounding monomer or polymer. The resulting organically-modified clay commonly is termed organoclay.

Despite such surface modification, it is still relatively difficult to achieve the exfoliated (homogeneously dispersed) structure that is thought to yield maximum enhancement of physical properties. Several types of idealized structures are possible within polymer–clay composite systems: poorly-dispersed composites (i.e. microcomposites) where no separation of the silicate layers has occurred; intercalated structures in which small increases in layer separation occur; and exfoliated structures containing completely separated and randomly oriented layers (Fig. 1). In many polymer–clay nanocomposites, a mixed structure is present, containing both intercalated and exfoliated nanostructures. In most in situ (bulk) polymerized PMMA–clay systems, the typical microstructures

* Corresponding author. Tel.: +61 2 9351 7526; fax: +61 2 9351 7682.
E-mail address: lisa.stadtmueller@emu.usyd.edu.au (L.M. Stadtmueller).

0032-3861/$ - see front matter © 2005 Elsevier Ltd. All rights reserved.
doi:10.1016/j.polymer.2005.08.036

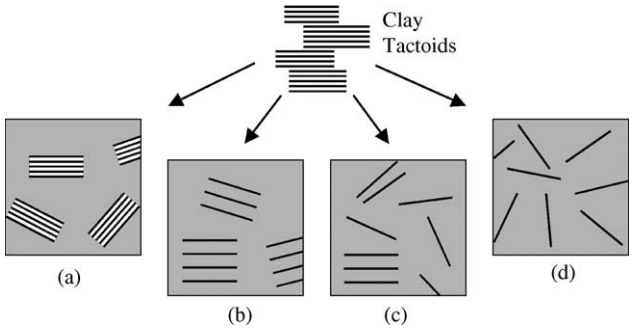

Fig. 1. Schematic depiction of the four types of idealized composite structures found in polymer–clay systems: (a) microcomposite, and (b) intercalated, (c) mixed and (d) exfoliated nanocomposites.

frequently are intercalated or mixed, rather than exfoliated, nanocomposites [10–12].

A more successful technique for improving layer dispersion involves modifying the platelet surfaces with specific organic cations that not only improve monomer compatibility but also initiate or catalyze polymerization from within the monomer-saturated tactoids [13]. This technique consistently has produced highly exfoliated nanocomposites in acid-catalyzed nylon and epoxy systems [14–17] as well as in metal-catalyzed polyolefin systems [18,19]. The success of this technique in increasing exfoliation is attributed to the shifting of the location of initiation from predominately extragallery (i.e. outside of the tactoids) to largely intragallery (i.e. within the tactoids). In these systems, the rate of intragallery initiation is increased by the presence of acidic onium ions or metal ions, which act as catalysts and cause the rate of polymerization within the spatially restrictive gallery of the clay to become competitive with the extragallery polymerization rates [13].

Unfortunately, this technique (in its current form) is not directly applicable to PMMA as polymerization of methylmethacrylate (MMA) is controlled by free radical initiation rather than acid or metal catalysis. Previous work by Park et al. attempted to indirectly adapt this technique to PMMA through epoxy aided dispersion of acidic-onium-ion-treated clay in epoxy/MMA mixtures [20]. However, their attempt was unsuccessful as the clay particles remained within the phase-separated epoxy domains and did not transfer to the PMMA. Thus, an intercalated, three-phase composite was formed with no clay in the PMMA phase. In order to more directly use this promising technique, a new approach for initiating free-radical-induced intragallery polymerization must be developed in order to improve layer dispersion in PMMA–clay systems.

Intragallery free radical initiation has been successfully achieved in styrene by Weimer et al. and Fan et al. via two different approaches [21,22]. Weimer et al. made use of nitroxyl-mediated living free radical polymerization, initiated from quaternized molecules that had been exchanged into the gallery region of a layered silicate [21]. Fan et al. quaternized the azo-initiator 2,2′-azobisisobutyronitrile (AIBN) to allow, after exchange into montmorillonite, intragallery free radical polymerization [22]. Both methods successfully yielded exfoliated nanocomposites; however, neither method included a compatiblizing agent within the gallery, so that each modified clay was an 'adsorptive' clay rather than a truly 'organophilic' clay [23]. Thus, in the case of Fan et al., extensive physical separation (i.e. stirring and sonication) was required to predisperse the treated clay within the monomer or monomer solution [22]. Furthermore, the initiators chosen for these studies were thermally activated and required lengthy periods of heating to polymerize. We have synthesized a novel molecule that is capable of improving monomer compatibility as well as catalyzing room temperature free radical polymerization within the gallery region, resulting in significantly more exfoliated PMMA–clay nanocomposites than those obtained from conventional organoclays.

2. Experimental section

2.1. Materials

Commercially available smectite clays were supplied by Nanocor Inc. as Nanomer® PGV, a sodium exchanged montmorillonite, and Nanomer® I.28EV, an octadecyltrimethylammonium (ODTMA) treated version of the same clay. Cloisite Na^+, a sodium exchanged montmorillonite from Southern Clay Products, was provided by Jim Chambers and Associates. The cation exchange capacity (CEC) of the Nanomer® PGV clay was reported by the supplier to be 130 mequiv/100 g; that of Cloisite Na^+ is 92 mequiv/100 g [24]. X-ray diffraction (XRD) comparisons of fractionated and unfractionated clays, followed by quantitative phase analysis with SIROQUANT software (Sietronics Pty. Ltd, Australia), indicated the as-received clay samples were montmorillonite with only minor quartz contamination; no other crystalline phases were detectable. Methyl methacrylate monomer (MMA) was purchased from Aldrich Chemical Co. containing 10–100 ppm monomethyl ether hydroquinone as inhibitor, which was removed through column separation. Initiators, benzoyl peroxide (BPO) from Fluka AG and *N*,*N*-dimethylanaline (DMA) from Aldrich Chemical Co., were used as received.

2.2. Synthesis of redox cationic surfactant

The novel redox cationic surfactant (RCS) was synthesized by the nucleophilic substitution reaction of 4,4′-methylenebis(*N*,*N*-dimethylaniline) with 1-bromooctadecane (both from Aldrich Chemical Co.), which were refluxed overnight in ethanol in the presence of silver nitrate. After cooling, the solution was filtered to remove silver nitrate, and water was added to separate the water-soluble co-quaternized byproduct from the less soluble

monoquaternized product. With the addition of water and gentle heating, the monoquaternized product coagulated and was filtered from the solution. The filtrate then was purified further by silica column chromatography with dichloromethane (DCM) as a flushing eluent. Because the desired product was cationic, it remained on the column until it was eluted with a 10:1:1 vol. mixture of DCM, methanol and nitromethane. The resulting product was confirmed by H_1 NMR spectroscopy to be *N*-4-(4′-*N*,*N*-dimethylaminophenyl)methylphenyl-*N*,*N*,-dimethyl-1-octadecanaminium nitrate (Fig. 2). The H_1 NMR spectrum of Fig. 2 confirms the molecular structure of the RCS, as it indicates the reduced symmetry of the molecule with substitution of only one of the nitrogens. Peaks 1 and 2 designate non-equivalent hydrogens on the aromatic rings. While the presence of two distinct peaks, 4 and 5 is indicative of different environments found near the methyl groups on the two nitrogens. The downfield shift of peak 4 is typical for charged amines. The group of peaks at 6 are associated with the hydrogens on the aliphatic tail.

2.3. Ion exchange of RCS onto clays

Due to the low water solubility of the RCS, the ion exchange process was carried out in a 78 wt% ethanol–water solution. The PGV and Cloisite Na clays were dried prior to weighing to reduce physically adsorbed water, before the desired quantity of clay was added to the ethanol solution at an approximate ratio of 1:200 by volume. A slight excess of RCS (1.05–1.10 times the CEC) was dissolved in ethanol solution with sonication and then was added slowly to the heated (45 °C) clay dispersions during mechanical mixing. The exchange reactions were continued for 24 h, after which the clays were washed three times with ethanol to remove displaced ions and excess RCS. The clays were oven dried at 60 °C and ground into fine powder with a mortar and pestle.

2.4. Polymerization of composites

Methacrylate–clay composites were prepared by mixing together two components. One component contained MMA with either the desired amount of RCS organoclay or the required amounts of I.28EV clay and DMA. These clay–MMA dispersions were sonicated for 20 min. The second component contained MMA and BPO at a BPO-RCS (or DMA) ratio of 2:1 wt%. Upon mixing of the two components with a vortex mixer for 30 s, free radical polymerization was initiated and a solid polymer was formed in approximately 1 h at room temperature.

2.5. Characterisation techniques

Thermogravimetric analysis (TGA), TA Instruments Hi-Res TGA 2950 (TA Instruments, Delaware, USA), was used to determine the organic content of the organoclays. Samples were run in high-resolution mode (resolution 5, sensitivity 1, initial heating rate of 50 °C/min) up to 1000 °C

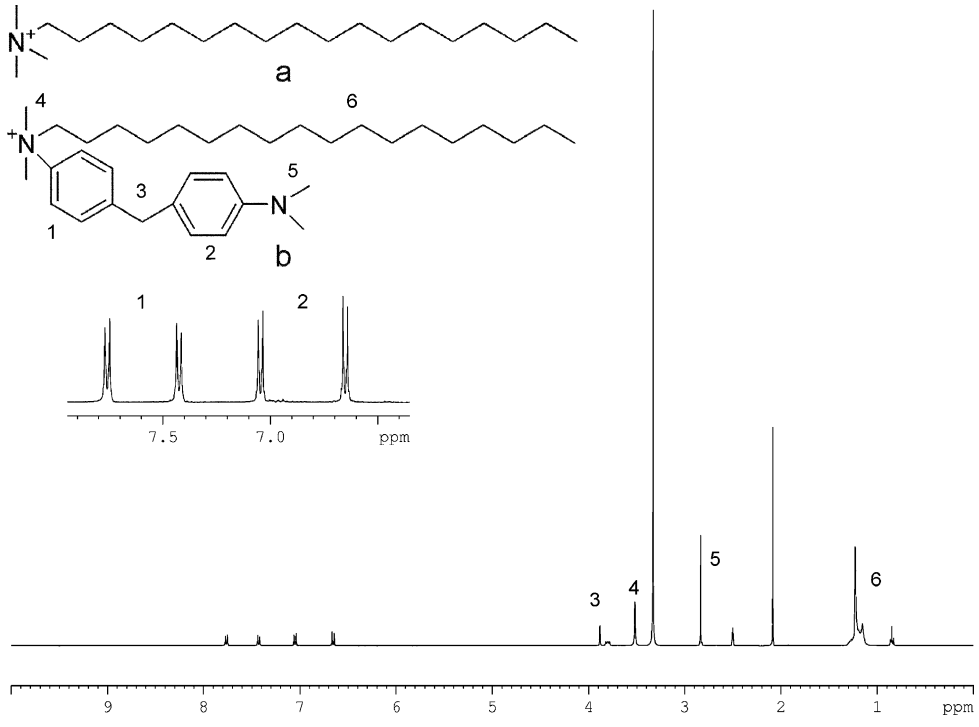

Fig. 2. The two types of organic cations used to modify the montmorillonite in this work: (a) the 18 carbon aliphatic chain surfactant ODTMA in the I.28EV organoclay; and (b) the corresponding novel redox cationic surfactant (RCS), which has an 18 carbon aliphatic chain and aromatic tertiary amine functionality. The H_1 NMR spectrum provides confirmation of the RCS molecule in (b).

in an O_2 atmosphere. To allow for the loss of structural water, the organic content was calculated as the difference between the mass lost by the organoclay and the mass lost by the corresponding untreated clay over the temperature range 150–900 °C. The accuracy of mass measurement of the TGA was reported by the manufacturer to be within ± 0.1%. Two or three replicates were made for each sample.

Powder XRD samples were prepared by packing clay into a 25 mm diameter metal holder. Liquid XRD samples were prepared in the same holder covered with 3.5 μm Hostaphan X-ray transparent film to reduce evaporation during measurement. Solid XRD samples were prepared by polymerizing the composites in a sealed, 24 mm-diameter glass mould. After polymerization, the glass was crushed and the solid disk was removed and polished to 6 μm finish with SiC grinding paper #4000. XRD analysis was performed on Siemens D5000 diffractometers (Siemens Pty. Ltd, Germany); for the liquid samples, and the corresponding nanocomposites, a diffractometer with a fixed stage and rotating source was used. Cu Kα X-rays were generated at 40 mA and 40 kV, and the angular (2θ) scanning rate and step size were 0.14°/min and 0.02°, respectively. For characterization of clays, samples were run over a 2θ range of 1–90°; this was reduced to 1–10° (2θ) for the solid nanocomposite samples.

Specimens for transmission electron microscopy (TEM) were prepared subsequently by cutting 5 mm slices off the polished solid disks. Ultrathin sections (<60 nm) were microtomed (Reichert Ultracut S, Leica) from these blocks with a diamond knife and then coated with carbon to reduce beam damage. TEM micrographs were obtained with a Zeiss 902 at 80 kV and a Philips CM120 at 120 kV.

3. Results and discussion

3.1. The architecture of RCS

At a molar ratio of 1.5:1 the nucleophilic substitution reaction of 1-bromooctadecane onto 4,4-methylene bis (*N*,*N*-dimethylanaline), which contains two identical tertiary amine sites, favors the quaternization of only one amine, leaving the other as an aromatic tertiary amine. The resulting cationic molecule was designed to mimic the long carbon chains of 18 carbons of the ODTMA molecules used in I.28EV organoclay, and contain an additional reactive aromatic tertiary amine capable of accelerating free radical polymerization (Fig. 2). The 18 carbon chain structure is used commonly in organoclays as it is within the range of favourable lengths (12–22 carbons) for expanding the interlayer distances and improving compatibility between the monomer and the normally hydrophilic clay surface [11,14]. The combination of BPO and aromatic tertiary amine is commonly used in dental restorative materials and bone cements to accelerate room temperature polymerization in the curing of acrylic resins [25]. Aromatic tertiary amines and BPO form a redox couple capable of accelerating free radical polymerization at room temperature [25–27]. This is accomplished with the formation of an intermediate coordination compound that increases the decomposition rate of BPO to generate free radical initiators [28]. Because the molecule is ion exchanged onto the clay surface, the amount of acceleration within the gallery is dependent upon the charge density of the clay and the amount of clay added to the system. The optimal ratio of BPO to amine was determined to be approximately 2:1 wt% by the method of Bowen et al., by reaction of MMA with free RCS and DMA [29]. As deliberate variations in the amount of RCS added to the system were necessary, due to the addition of different types and/or amounts of RCS-modified clay, the optimal ratio of 2:1 wt% was kept constant throughout all the experiments by varying the concentration of BPO added.

3.2. Characterisation of organoclays

The successful modification of the clays is shown by the large shifts in basal peak position of the treated clays with respect to the as-received montmorillonites (Table 1 and Fig. 3). These shifts are indicative of gallery expansion due to the presence of RCS molecules within the gallery regions. In the case of the commercial organoclay I.28EV, the basal spacing listed in Table 1 and the absence of an integral (00*l*) series (full XRD data not shown) suggest an interlayer structure that is a mixture of pseudotrimolecular and paraffin-type galleries. For the RCS organoclays, although the basal spacings were reasonably similar to that of I.28EV and there were no integral (00*l*) series, the packing structure

Table 1
Compilation of data relating to the exchange of the treated clays

Organoclay	Molar mass of modifier (g/mol)	CEC of clay (mequiv/100 g)	Untreated $d_{(001)}$ (nm)	Treated $d_{(001)}$ (nm)	Organic content[a] (%)	Amount of CEC exchanged[b] (%)	Estimated area per unit charge[c] (nm^2)
I.28EV	312.6	130	1.3	2.4	28.5±0.1	95±3	0.97
PGV-RCS	507.9	130	1.3	2.9	32.6±0.8	71±4	0.97
Clo-RCS	507.9	92	1.3	2.3	26.3±0.8	75±2	1.36

[a] Values were calculated from TGA data; reported error is the reproducibility across replicate samples or instrumental error, whichever is larger.
[b] Values calculated from the organic content and CEC.
[c] Interpolated from data of Laird on CECs of smectites versus interlayer charge [38].

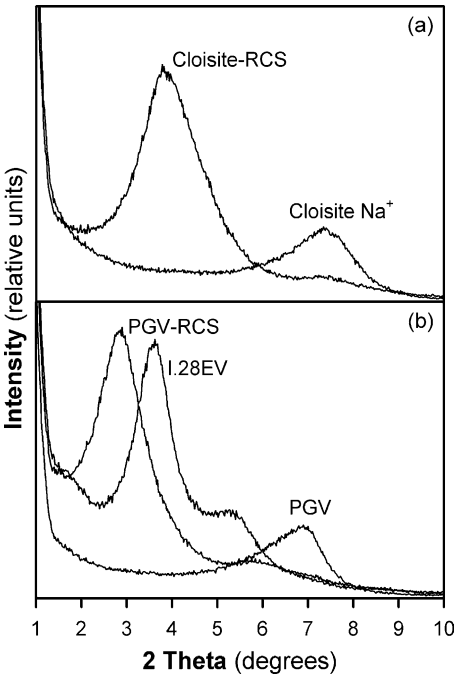

Fig. 3. XRD patterns of sodium clays versus organoclays. The shifts in peak position indicate interlayer expansion caused by the presence of organic cations in the galleries.

is complicated by the presence of the aromatic portions of the molecules.

Further complications in interpreting the interlayer structure arise from the incomplete exchange of the PGV and Cloisite clays. Unlike the near stoichometrically-exchanged I.28EV organoclay, the organic contents of the treated clays (Table 1) indicate that the RCS molecules exchanged on only approximately 75% of available exchange sites on the low and high CEC clays. Such incomplete cation exchange might be attributed to two main factors. Firstly, the larger size and unusual shape of the RCS molecule compared with the ODTMA molecule might have caused the exchanged molecules to physically block a proportion of the possible exchange sites, thereby preventing complete exchange. Secondly, although the commercial exchange conditions used during the manufacture of I.28EV are not known, it seems likely that differences in the exchange conditions—such as exchange solvent, temperature, solubility of the modifier and the amount of excess modifier in solution—could account for the lower exchange in the RCS treated samples. However, given that the RCS content remained approximately constant across the two organoclays, even though the surface area per exchange site differed significantly (Table 1), it seems likely that issues related to differences in exchange conditions and the low solubility of the RCS controlled the exchange process more than molecular size.

This suggestion is supported by analysis of the projected areas occupied by the RCS molecules in the interlayer regions. Following the usual model for the packing of alkylammonium molecules between smectite layers, the alkyl tails were assumed to maintain a rigid, all trans conformation [30–32]. In this way, pairs of RCS molecules can pack with their alkyl tails together, the cationic nitrogens at opposite ends of the molecular pair and facing out to the negatively charged platelets, and the aromatic groups curving away from these surfaces and around the tail ends of the neighbouring molecules. Space-filling, molecular models of this structure were created in Spartan'04 Essential 2.0.0 (Wavefunction Inc., Irvine, CA, 2003) and distances and areas measured in analySIS Pro 3.2 (Soft Imaging System GmbH, Münster, Germany, 2002). With the paired tails as flat to the platelets as possible—the presence of the aromatic groups prevents a completely parallel arrangement—this basic repeating unit approximates a bilayer structure of thickness 1.4 nm. Allowing a small amount of keying of the quaternary group into the ditrigonal cavities of the platelets, which have a thickness of 0.95 nm [33], the 2.3 nm basal spacing of the Clo-RCS organoclay is obtained. Tilting the pairs of molecules away from the platelets to a tilt angle of approximately 16° generates a basal spacing of 2.9 nm, corresponding to the PGV-RCS organoclay. The projected areas occupied by these molecular arrangements were measured (analySIS Pro 3.2), and the area per single molecule is 0.88 or 0.91 nm^2, both of which are less than the smallest estimated area per unit charge of the two clays at 0.97 nm^2. Recognising that, owing to layer charge heterogeneity, some layers in the PGV clay would have smaller areas per unit charge than 0.97 nm^2, but also recognising that the actual RCS molecules would adopt more flexible and, therefore, more compact arrangements, it seems that the RCS molecules are unlikely to have prevented complete exchange by physically blocking exchange sites. As suggest above, the low solubility and/or small excess of the RCS molecules during exchange are more likely culprits.

The result of this incomplete exchange of the RCS organoclays is that these systems would contain significant amounts (approximately 25%) of residual Na^+ ions; Shi et al. found residual Na^+ in organoclays produced by single exchange with propylammonium or octylammonium ions, even though near stoichometric exchange was achieved (91–99%) [34]. If the 25% of residual Na^+ ions in the RCS organoclays are uniformly distributed among the organoclay interlayers then they are likely to have little impact on the swelling of the organoclays, although clearly they mean that 25% fewer tertiary amines are available to initiate intragallery polymerisation than if the organoclays were stoichiometrically exchanged. However, if some or all of the Na ions are segregated into separate galleries, the resulting interstratified structure would contain both swelling (RCS) and non-swelling (Na^+) galleries; the latter also would be unable to generate any intragallery initiation. To determine which of these two structures—mixed or interstratified—predominated in the organoclays, the MacEwan direct Fourier transform was applied to the experimentally

measured diffraction peaks of the organoclays [35]. Based on the molecular models discussed above, the structure factors for pure montmorillonite platelets with (1) pure Na^+ galleries, (2) pure RCS galleries and (3) homogeneously-mixed RCS-Na galleries were calculated and used to determine the transforms as described by Reynolds [35]. However, neither the mixed nor the interstratified models were found to produce a Fourier transform that was consistent with either model. This is likely to be due to the few major diffraction peaks in the experimental data (only five or six reasonable peaks) and possibly also due to the departure of the real interlayer structures in the RCS organoclays from the basic 'all-trans' models used here [36,37]. Consequently, it is not possible to draw a definitive conclusion as to the arrangement of the residual Na^+ across the organoclay interlayer environments. Still, the absence of any significant peaks in the organoclay diffraction data at or near the basal spacings of the parent montmorillonites (1.3 nm) suggests that the majority of residual Na^+ probably is randomly distributed with the RCS molecules across all the galleries, rather than segregated in pure Na^+ interlayers. (The very small peaks adjacent to the basal peaks for both organoclays are most likely 002 reflections, given their angular values.) Therefore, it is anticipated that the presence of the residual Na^+, though not ideal for maximum reactivity, should not interfere with the desired intragallery initiation in the RCS organoclays by formation of organophobic, completely unreactive interlayers. As is presented below, this expectation is borne out in the nanocomposite samples made from these RCS organoclays,

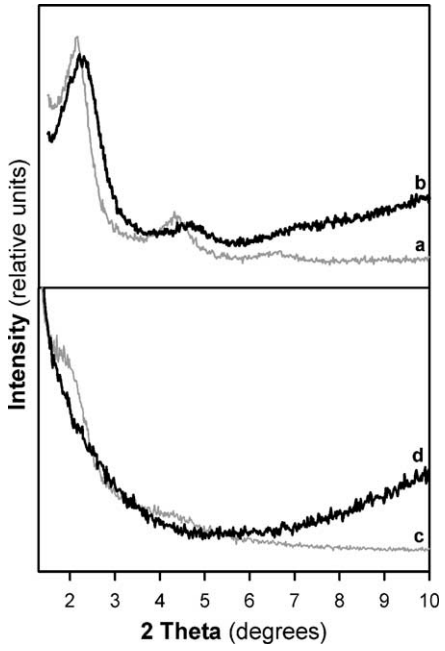

Fig. 4. XRD patterns of I.28EV treated clay and PGV-RCS treated clay in unpolymerized MMA and in polymerized PMMA: (a) I.28EV in monomer; (b) I.28EV in polymer; (c) PGV-RCS in monomer; (d) PGV-RCS in polymer. All samples contained 3.60±0.03 wt% clay.

which showed an absence of any basal peaks when characterised by XRD. This is indirect evidence for the random distribution of the residual Na^+ ions in the galleries of the RCS organoclays; large amounts (~25%) of segregated Na^+ galleries would not have delaminated and, therefore, would have been detectable by their small basal peaks at higher-angles.

3.3. Effect of gallery-localized aromatic tertiary amine on nanocomposite morphology

Fig. 4 compares XRD patterns of unpolymerized and polymerized dispersions of the I.28EV and PGV-RCS organoclays. When I.28EV was added to the uncured MMA the monomer was adsorbed in between the clay layers and the interlayer distance was expanded significantly (Fig. 4); the shift in peak position indicated the mean interlayer distance, $d_{(001)}$, changed from 2.4 to 4.1 nm. Upon polymerization of the dispersion of I.28EV in MMA with the addition of BPO and DMA, the interlayer distance was reduced to 4.0 nm. Although the I.28EV was compatible with the monomer (as indicated by significant swelling of the galleries), the small reduction in interlayer spacing during polymerization suggests that improving compatibility is not the only factor influencing platelet dispersion. This same phenomenon of partial gallery collapse upon polymerization of clay–monomer dispersions also has been observed in similar systems [10,39]. One possible explanation for this occurrence is the role of large extragallery polymerization rates on nanocomposite morphology. It has been suggested that in a system with predominantly extragallery polymerization, the adsorbed monomer leaves the interlayer space and becomes involved in the external polymer propagation, resulting in reduced interlayer distances [13,39]. It should be possible to validate this theory for the PGV-RCS organoclay system, in which the modifier is designed to produce an organophilic clay and also increase the rate of intragallery polymerization.

When PGV-RCS organoclay was dispersed in the monomer, XRD patterns again revealed shifts in peak position from the large peak at 2.9 nm (Fig. 3) to a low intensity peak at 4.3 nm (Fig. 4(c)). Because the monomer was adsorbed within the layers of the I.28EV and PGV-RCS clays, compatibility was evident in both systems. Thus, the goal of producing good compatibility for RCS-modified clay has been achieved. Upon the addition of BPO to this system, it was expected that, if diffusion of BPO into the galleries was not sterically hindered, the aromatic tertiary amine groups of the RCS molecules would accelerate the decomposition of BPO and, thus, initiate near-surface, intragallery polymerization. This was found to be the case in practice, because (1) polymerization occurred quite rapidly upon addition of BPO and (2) the resulting interlayer spacing of the polymerized sample was greater than 7 or 8 nm, as shown by the absence of Bragg scattering in Fig. 4(d) (the upper limit for determination of intragallery

spacing in XRD with Cu Kα radiation is at most 8 nm). The expansion of the galleries in the intragallery initiated system supports the previous explanation for the reduction of interlayer distance in the I.28EV system during polymerization; i.e. too large extragallery (or too small intragallery) polymerization rates.

The foregoing XRD data (Fig. 4(b) and (d)) indicate that the I.28EV and PGV-RCS nanocomposite samples were intercalated and exfoliated, respectively, at least based on the XRD definition of exfoliation. Visual comparison of low magnification TEM images of the two composites confirms the substantial improvement of clay dispersion and the decrease in particle size for the PGV-RCS system over that of the I.28EV system (Fig. 5). However, close inspection of high magnification TEM images (presented later) indicates that complete exfoliation has not been achieved because small tactoids, containing on average 3–5 layers, remain dispersed throughout the composite structure.

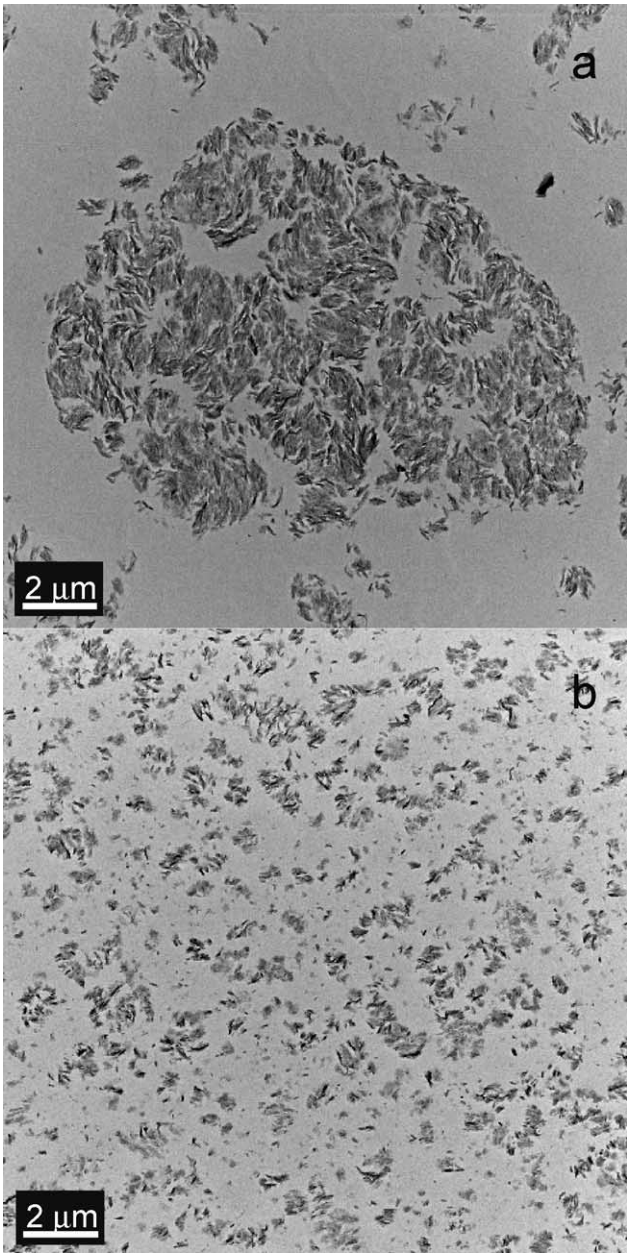

Fig. 5. Brightfield TEM images of polymerized methylmethacrylate–clay dispersions at 3.60±0.03 wt% clay loading: (a) I.28EV organoclay and (b) PGV-RCS organoclay.

3.4. Effects of extragallery and intragallery polymerization rates

From their extensive work in epoxy systems, Lan and coworkers concluded that maximizing the degree of exfoliation in polymer–clay nanocomposites requires not just an increase in intragallery polymerization rates, but actual optimization of the relative extragallery and intragallery polymerization rates [14]. Therefore, it seems probable that the balance between these polymerization rates also would influence the final nanocomposite morphology in the PMMA systems under examination here. Practically, it is not possible to measure the local rates of extragallery versus intragallery polymerization at present. Consequently, it is difficult to conclusively establish what is actually happening with the relative rates of local polymerization within the systems discussed above.

Nonetheless, given that BPO decomposition also is regulated thermally, it was considered probable that the exotherm produced during polymerization was sufficient to partially decompose the externally located BPO and cause some extragallery initiation during polymerization in the PGV-RCS system. To gain some qualitative insight into the significance of this effect, a dispersion of RCS-treated clay in MMA, with added BPO, was heated in an oven at 65 °C to accelerate the pervasive thermal-decomposition of the BPO while allowing the localized, RCS-induced decomposition of BPO to continue in the galleries. For brevity, neither the XRD nor TEM results for this sample are presented, but both revealed the detrimental effect of heat-induced acceleration of extragallery polymerisation on degree of exfoliation. The XRD showed the reappearance of a small basal peak at approximately 3.5 nm; the TEM micrographs exhibited a significant increase in microstructural heterogeneity and coarsening. This result is not surprising, given that elevated temperatures accelerate decomposition of BPO and, therefore, were expected to increase the rate of extragallery polymerization. However, it does indicate that the magnitude of extragallery polymerization generated by the exotherm in the room temperature reaction is far below the increased extragallery polymerization rate caused by heating to 65 °C.

In an attempt to more quantitatively regulate the relative rates of polymerization in the RCS organoclay system, a second aromatic tertiary amine, DMA, was added to accelerate the decomposition of BPO outside the galleries so that both extra and intragallery polymerization were initiated at room temperature. The amount of externally added DMA was varied while the internal aromatic tertiary

amine (RCS) and BPO amounts were held constant. The resultant XRD patterns of the polymerized composites showed increasing levels of Bragg scattering (i.e. increasing peak size) with increasing concentrations of DMA (Fig. 6). Clearly, increasing the rate of extragallery polymerization with the externally added DMA reduced delamination of the clay. The TEM images presented in Fig. 7 confirm this phenomenon, as improvements in dispersion are visible with a reduction in DMA concentration. It is evident that the original sample without added DMA produced the highest degree of exfoliation; therefore—of the systems with varying concentration of intragallery and extragallery initiators examined here—it has the optimal balance between intragallery and extragallery polymerization rates. Even though the actually intragallery and extragallery polymerization rates are not known, this is suggestive that the optimal balance in this system is one of where intragallery polymerization predominates and extragallery polymerization is small.

3.5. Effects of layer charge density

In polymer–clay nanocomposite systems, the layer charge density of the clay influences a number of factors that ultimately affect the degree of exfoliation. Frequently referred to in terms of the CEC—a closely related, but not equivalent, parameter—the layer charge density per platelet controls the packing geometry of the interlayer modifier cations, the degree of surface coverage by those cations and the overall interlayer distance in organoclays (Table 1). These factors affect the amount of monomer adsorption within the clay, as well as the magnitude of the attractive electrostatic forces that must be overcome during delamination. Thus, it is not surprising that in intragallery-catalyzed epoxy systems it was found that the CEC of the clay strongly influenced the degree of layer exfoliation [14].

To investigate this effect in the PMMA system, we compared two RCS-treated organoclays made from montmorillonites possessing high and low CECs of 130 mequiv/100 g and 92 mequiv/100 g: the original PGV-RCS organoclay and the Clo-RCS organoclay, respectively. The absence of Bragg scattering in the XRD patterns (not shown) of the PMMA–clay nanocomposites made from both organoclays indicates layer separations exceeding 7 or 8 nm in each system. Clearly, this suggests a significant level of exfoliation in both samples; however, the morphology of the nanocomposites cannot be distinguished

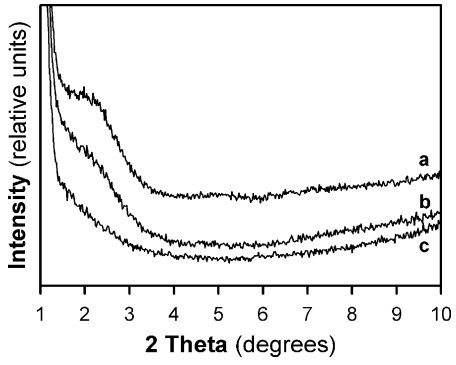

Fig. 6. XRD patterns of polymerized composites containing: (a) 5.28 wt% PGV-RCS treated clay and 1.5 wt% externally added DMA; (b) 5.28 wt% PGV-RCS treated clay and 0.75 wt% of externally added DMA; and (c) 5.28 wt% PGV-RCS treated clay only. 3.3 wt% BPO was added to all mixtures.

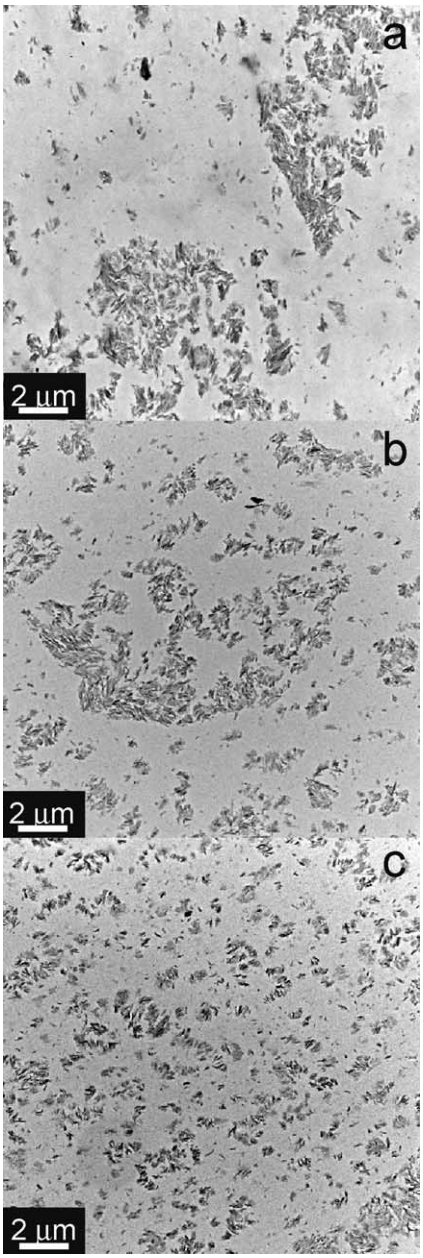

Fig. 7. TEM images of polymerized composites containing: (a) 5.28 wt% PGV-RCS treated clay and 1.5 wt% externally added DMA; (b) 5.28 wt% PGV-RCS treated clay and 0.75 wt% of externally added DMA; and (c) 5.28 wt% PGV-RCS treated clay only. 3.3 wt% BPO was added to all mixtures.

on this basis, so that a comparison of TEM images is necessary instead (Fig. 8).

The low magnification TEM images reveal a large difference in tactoid morphology: the high CEC organoclay produced compact particles (Fig. 8(a)); the low CEC organoclay produced more elongated particles (Fig. 8(e)). This difference in structure, suggests differences in mean platelet length, and the high magnification images (Fig. 8(d) and (h)) support this suggestion. Thus, although the low magnification images (Fig. 8(a) and (b)) provide a reasonably representative sampling of the microstructures of the nanocomposites, the possible effects of CEC on morphology are confounded with the effects caused by differences in platelet size. Moreover, because individual platelets cannot be seen at this magnification, it is difficult to assess the degree of exfoliation. With higher magnifications, platelet visibility increases, more clearly revealing the degree of exfoliation among the individual platelets, however, the sampling area (projected volume) simultaneously becomes smaller. Consequently, at the highest magnification presented here, it would be questionable to select a single field area of less than 0.5 μm^2 for each sample and regard them as representative of the entire morphology of the samples. A comparison of differing degrees of dispersion from such single, high magnification images alone is subject to sizable error and dependent upon observational interpretation. This difficulty illustrates the need for image analysis approaches that can be used to provide quantitative measures of nanocomposite structure across sufficiently large sample sets that any conclusions drawn have an adequate level of statistical confidence. We are doing ongoing work in this area. For the purposes of this study, however, it is sufficient to estimate the relative degrees of exfoliation by manual counting processes. To that end, the number of layers and tactoids visible in six representative TEM images (85,000× magnification such as in Fig. 8(c) and (g)) were counted for both samples (total layers counted of 648 and 939, respectively for the Clo-RCS and PGV-RCS nanocomposites). From this preliminary analysis, it was found that the mean number of layers per tactoid—1.58 for Clo-RCS and 1.76 for PGV-RCS—was smaller and the mean degree of exfoliation—i.e. number of single layers divided by total number of layers; 47% for Clo-RCS to 37% for PGV-RCS—was larger for the Clo-RCS than the PGV-RCS nanocomposite. This simple analysis suggests that the lower CEC organoclay produced a measurably higher degree of exfoliation. This tentative finding accords with the results of Lan et al. [14]. The data for both samples also shows that, as was mentioned earlier, the use of the RCS-modified clays significantly increases, but does not achieve full, exfoliation. Perhaps the main point to note here, however, is the difficulty in drawing any definitive conclusions without this type of analysis, and the need for improved means of quantifying differences in morphology in polymer–clay nanocomposite systems.

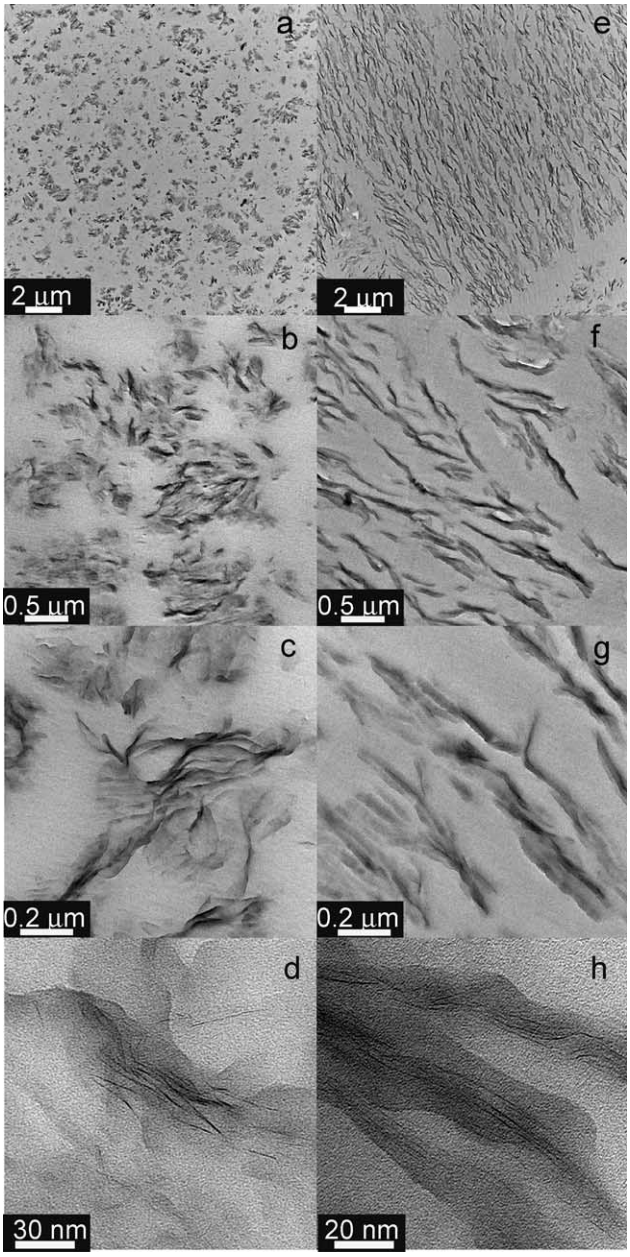

Fig. 8. Typical brightfield TEM images of PMMA–clay nanocomposites containing: high CEC clay (PGV-RCS organoclay) ((a)–(d)) and low CEC clay (Clo-RCS organoclay) ((e)–(h)). All samples contained 3.60 ± 0.03 wt% clay.

4. Conclusions

Surface modification of montmorillonite clay is essential for aiding the homogeneous dispersion of platelets throughout the polymer matrix in polymer–clay nanocomposite systems. Ion exchanging aliphatic cations within the gallery region increases compatibility and monomer absorption, however, it is not sufficient to exfoliate clay in bulk polymerized PMMA–clay composites. Rather, accelerating intragallery polymerization over extragallery

polymerization with the addition of aromatic tertiary amine groups as part of a redox couple initiates near-surface free radical polymerization within the gallery region and significantly improves platelet dispersion. A balance must be maintained between the intragallery and extragallery polymerization rates to optimize expansion. If extragallery polymerization is favored, either by thermal or chemical acceleration, reduction in interlayer spacing occurs during the polymerization process. The CEC of the clay also influences the degree of dispersion. Based on data from limited, manual image analysis of TEM images, the lower CEC organoclay produces more exfoliated nanocomposites, although new methods to quantify differences in dispersion must be developed for further substantiation. With the synthesis of a novel molecule, we have developed a successful method for significantly increasing exfoliation of clay in free radical room temperature polymerization of PMMA–clay nanocomposites. One notable aspect of this new compound is that it does impart color to the normally clear and transparent polymer. This is common to amine/BPO redox couples, but might be altered with further modification of the RCS molecular structure.

Acknowledgements

This research was supported by The Australian Key Centre for Microscopy and Microanalysis in conjunction with the Key Centre for Polymer Colloids (KCPC) at The University of Sydney. Both centres were established and are supported under the Research Centres Program of the Australian Research Council (ARC). We also acknowledge the generous donation of clay materials by Nanocor, Inc. and Jim Chambers and Associates. Special thanks go to Prof Maxwell Crossley, Dr Pall Thordarson and Dr Iain Blake for their helpful advice on the RCS synthesis and purification. Constructive contributions by Prof Robert G. Gilbert of the KCPC are also gratefully acknowledged. Dr Ian Luck is thanked for assistance with interpretation of the H_1 NMR spectrum of the RCS molecule.

References

[1] Lan T, Pinnavaia TJ. Clay-reinforced epoxy nanocomposites. Chem Mater 1994;6:2216–9.
[2] Al-Esaimi MM. Reaction catalyzed by montmorillonite: polymerization of methyl methacrylate. J Appl Polym Sci 1997;64:367–72.
[3] Chen GH, Yao KD, Zhao JT. Montmorillonite clay/poly(methyl methacrylate) hybrid resin and its barrier property to the plasticizer within poly(vinyl chloride) composite. J Appl Polym Sci 1999;73:425–30.
[4] Fu X, Qutubuddin S. Polymer–clay nanocomposites: exfoliation of organophilic montmorillonite nanolayers in polystyrene. Polymer 2001;42:807–13.
[5] Huang J-C, Zhu Z-K, Ma X-D, Qian X-F, Yin J. Preparation and properties of montmorillonite/organo-soluble polyimide hybrid materials prepared by a one-step approach. J Mater Sci 2001;36:871–7.
[6] Zhu J, Wilkie CA. Thermal and fire studies on polystyrene–clay nanocomposites. Polym Int 2000;49:1158–63.
[7] Zhu J, Morgan AB, Lamelas FJ, Wilkie CA. Fire properties of polystyrene–clay nanocomposites. Chem Mater 2001;13:3774–80.
[8] Alexandre M, Dubois P. Polymer-layered silicate nanocomposites: preparation, properties and uses of a new class of materials. Mater Sci Eng, R 2000;28:1–63.
[9] Ratinac KR, Zhu HY, Stadtmueller LM, Ringer SP. Case studies in nanostructural analysis for understanding nanomaterials. Mater Forum 2002;26:44–73.
[10] Okamoto M, Morita S, Taguchi H, Kim YH, Kotaka T, Tateyama H. Synthesis and structure of smectic clay/poly(methyl methacrylate) and clay/polystyrene nanocomposites via in situ intercalative polymerization. Polymer 2000;41:3887–90.
[11] Chen G, Yao K, Zha J. Montmorillonite clay/poly(methyl methacrylate) hybrid resin and its barrier property to the plasticizer within poly(vinyl chloride) composite. J Appl Polym Sci 1999;73:425–30.
[12] Wang D, Zhu J, Yao Q, Wilkie CA. A comparison of various methods for the preparation of polystyrene and poly(methyl methacrylate) clay nanocomposites. Chem Mater 2002;14:3837–43.
[13] Pinnavaia TJ, Beall GW. In: Scheirs J, editor. Polymer–clay nanocomposites. New York: Wiley; 2000.
[14] Lan T, Kaviratna PD, Pinnavaia TJ. Mechanism of clay tactoid exfoliation in epoxy–clay nanocomposites. Chem Mater 1995;7:2144–50.
[15] Okada A. The processing and properties of a nylon 6/clay hybrid. JOM 1993;45:71.
[16] Okada A, Usuki A. The chemistry of polymer–clay hybrids. Mater Sci Eng, C, Biomimetic Mater Sens Syst 1995;3:109–15.
[17] Wang Z, Lan T, Pinnavaia TJ. Hybrid organic–inorganic nanocomposites formed from an epoxy polymer and a layered silicic acid (magadiite). Chem Mater 1996;8:2200–4.
[18] Bergman JS, Chen H, Giannelis EP, Thomas MG, Coates GW. Synthesis and characterization of polyolefin–silicate nanocomposites: a catalyst intercalation and in situ polymerization approach. Chem Commun 1999;2179–80.
[19] Heinemann J, Reichert P, Thomann R, Mulhaupt R. Polyolefin nanocomposites formed by melt compounding and transition metal catalyzed ethene homo- and copolymerization in the presence of layered silicates. Macromol Rapid Commun 1999;20:423–30.
[20] Park JH, Jana SC. The relationship between nano- and microstructures and mechanical properties in PMMA–epoxy-nano clay composites. Polymer 2003;44:2091–100.
[21] Weimer MC, Chen H, Giannelis EP, Sogah DY. Direct synthesis of dispersed nanocomposites by in situ living free radical polymerization using a silicate-anchored initiator. J Am Chem Soc 1999;121:1615–6.
[22] Fan X, Xia C, Advincula RC. Grafting of polymers from clay nanoparticles via in situ free radical surface-initiated polymerization: monocationic versus bicationic initiators. Langmuir 2003;19:4381–9.
[23] Nzengung VA, Voudrias EA, Nkedi-Kizza P, Wampler JM, Weaver CE. Organic cosolvent effects on sorption equilibrium of hydrophobic organic chemicals by organoclays. Environ Sci Technol 1996;30:89–96.
[24] Yoon PJ, Hunter DL, Paul DR. Polycarbonate nanocomposites. Part 1. Effect of organoclay structure on morphology and properties. Polymer 2003;44:5323–39.
[25] Brauer GM, Argentar H. Initiator–accelerator systems for dental resins. ACS Symp Ser 1983;212:359–71.
[26] Elvira C, Levenfeld B, Vazquez B, San Roman J. Amine activators for the 'cool' peroxide initiated polymerization of acrylic monomers. J Polym Sci, Part A: Polym Chem 1996;34:2783–9.
[27] Vazquez B, Levenfeld B, San Roman J. Role of amine activators on the curing parameters, properties and toxicity of acrylic bone cements.. Polym Int 1998;46:241–50.

[28] Brauer GM, Davenport RM, Hansen WC. Accelerating effect of amines on polymerization of methyl methacrylate. Mod Plast 1956; 34:153–4 [see also p. 156–8, 163–4, 166, 168, 256].
[29] Bowen RL, Argentar H. Method for determining the optimum peroxide-to-amine ratio for self-curing resins. J Appl Polym Sci 1973; 17:2213–22.
[30] Lagaly G. Interaction of alkylamines with different types of layered compounds. Solid State Ionics 1986;22:43–51.
[31] Lagaly G, Weiss A. In: Heller L, editor. Proceedings of the international clay conference. Tokyo: Israel Universities Press; 1969. p. 61–80.
[32] Slade PG, Gates WP. The swelling of HDTMA smectites as influenced by their preparation and layer charges. Appl Clay Sci 2004;25:93–101.
[33] Fornes TD, Paul DR. Modeling properties of nylon 6/clay nanocomposites using composite theories. Polymer 2003;44: 4993–5013.
[34] Shi H, Lan T, Pinnavaia TJ. Interfacial effects on the reinforcement properties of polymer–organoclay nanocomposites. Chem Mater 1996;8:1584–7.
[35] Brindley GW, Brown G, editors. Mineralogical society monograph. Crystal structures of clay minerals and their X-ray identification, vol. 5.
[36] Vaia RA, Teukolsky RK, Giannelis EP. Interlayer structure and molecular environment of alkylammonium layered silicates. Chem Mater 1994;6:1017–22.
[37] Hackett E, Manias E, Giannelis EP. Molecular dynamics simulations of organically modified layered silicates. J Chem Phys 1998;108: 7410–5.
[38] Laird DA. Layer charge influences on the hydration of expandable 2:1 phyllosilicates. Clays Clay Miner 1999;47:630–6.
[39] Akelah A, Kelly P, Qutubuddin S, Moet A. Synthesis and characterization of ‘epoxyphilic’ montmorillonites. Clay Miner 1994;29:169–78.